Electric-field effects on the closed orbits of the diamagnetic Kepler problem

C. Bleasdale[*]
Institute for Superconducting and Electronic Materials and School of Physics, University of Wollongong, New South Wales 2522, Australia

A. Bruno-Alfonso[†]
Departamento de Matemática, Faculdade de Ciências, Unesp - Universidade Estadual Paulista, Bauru, São Paulo 17033-360, Brazil

R. A. Lewis[‡]
Institute for Superconducting and Electronic Materials, School of Physics and Faculty of Engineering and Information Sciences, University of Wollongong, New South Wales 2522, Australia

(Received 23 July 2015; revised manuscript received 8 November 2015; published 5 February 2016)

The nonrelativistic closed orbits of an electron interacting with a unit positive charge in the presence of homogeneous magnetic and electric fields are investigated. A simplified theoretical model is proposed utilizing appropriate initial conditions in semiparabolic coordinates for arbitrary magnetic- and electric-field alignments. The evolution of both the angular spectrum of orbits and the shape and duration of individual orbits, as the electric-field intensity and scaled energy are increased, is shown for the cases of both parallel and crossed fields. Orbit mixing in the high-field regime is investigated in the case of parallel fields, giving an indication of the system moving from the quasi-Landau chaotic regime to the electric-field-induced (Stark effect) regular regime. For crossed fields, it is shown that the Garton-Tomkins orbits lead to a pair of orbits that have opposite behaviors as a function of the electric-field intensity.

DOI: 10.1103/PhysRevA.93.023405

I. INTRODUCTION

The study of the hydrogen atom, and other atomic species, in external fields as experimentally accessible quantum systems whose classical analog displays chaotic properties has been pursued extensively for many decades [1–4]. In a static magnetic field, the system is known to be chaotic at energies around the ionization point. This chaotic behavior manifests itself in experimental measurements as oscillations in the spectrum whose periods correspond to the periods of closed orbits in the classical Hamiltonian [5].

The addition of a static electric field parallel to the magnetic field provides another system which is both experimentally accessible and able to be solved analytically in the classical case [6–8]. In this configuration, the symmetry of the system is preserved with the z component of the angular momentum of the system remaining conserved. Therefore, calculations are relatively simple when compared to the general case. The integrals of motion of hydrogenic atoms in the presence of parallel magnetic and electric fields has been investigated by Beims and Gallas [9]. The chaotic ionization of the same system has been studied by Topçu and Robicheaux [10]. In the extreme case of a pure electric field, there exists an exact quantum solution due to the separability of the Schrödinger equation. Therefore, the classical motion in this system is regular everywhere [11–13]. By applying both fields at varying comparable strengths we are able to observe the system evolving from regular to chaotic dynamics [6,8].

By rotating the electric field away from parallel to the crossed-fields geometry, the conservation of the z component of the angular momentum of the system is broken and calculations become more complicated. The closed orbits of an electron in a hydrogen atom in crossed fields have been studied by several authors [14–19]. In particular, the graphs of a set of orbits with a negative energy value have been reported by Rao *et al.* [20,21]. To remove the Coulomb singularity, they combined the Kustaanheimo-Stiefel transformation with a time-dilation variable in the four-dimensional representation.

Much of the work dedicated to these three cases has been concentrated on energies less than or at the ionization threshold as this is convenient for experimental data gathered in hydrogen and other atomic systems. Recently, however, the diamagnetic Kepler problem was first detected in the semiconductor environment of silicon in a static magnetic field [22]. The oscillations in the spectrum were observed well above the ionization threshold corresponding to positive scaled energies of the order of 1 [23]. These measurements also provided an observation of this effect in an anisotropic medium which subsequently led to a comprehensive study on the effects of an anisotropic mass on the classical electron orbits and their periods [23]. A numerical investigation into the experimental conditions needed to observe such an effect in a range of widely-utilized semiconductors was also completed [24].

In the present work, the effect of an electric field which is either parallel or perpendicular to the magnetic field applied to a hydrogenic atom is further investigated. Section II provides the classical theoretical framework for a three-dimensional (3D) hydrogenic atom in both magnetic and electric fields at arbitrary orientation. The singularity at the nucleus is softened using scaled semiparabolic coordinates and the choosing of appropriate initial conditions. Such a choice allows us to deal with a more general configuration than previous works restricted to the 2D hydrogen atom [25–27]. Relevant equations of motion for the special cases of parallel and crossed

[*]cb123@uowmail.edu.au
[†]alexys@fc.unesp.br
[‡]roger@uow.edu.au

 ©2016 American Physical Society

fields are presented. Section III outlines the numerical results for parallel and crossed fields. In each case, a systematic investigation is detailed on both the angular spectrum of orbits, as well as the shapes and periods of the most important closed orbits as the scaled field is increased. In the case of parallel fields, two further investigations are presented. The first focuses on orbit mixing in the high-field regime between orbits associated with quasi-Landau oscillations and the single electric-field-induced orbit associated with the Stark effect. This describes how the system shifts from the chaotic quasi-Landau regime to the regular electric-field-induced orbits regime, and how this mixing of orbits can create large regions of the angular spectrum where closed orbits are abundant. Such a large region of closed orbits may lead to strong oscillations in the spectrum related to those specific orbit periods. The second considers the effects of small positive integer values of the scaled energy on both the angular spectrum of orbits, as well as the shapes and periods of the most important closed orbits. This is of particular interest when moving into the semiconductor environment where experimental work has shown oscillations in the spectrum well above the ionization energy [22–24]. For crossed fields, it is shown how the electric field breaks the rotational symmetry, splitting the shortest pure magnetic orbits into new ones which evolve quite differently as the field strength is increased. The evolution of other orbits is discussed as well. Section IV provides a summary of the important results and conclusions.

II. THEORETICAL FRAMEWORK

The diamagnetic Kepler problem deals with an electron of mass m and charge $-e$ interacting with a positive charge e in the presence of a magnetic field $\boldsymbol{B}$. The frequency of the cyclotron motion of the electron in such a field is given by $\omega_c = eB/m$. When an electric field $\boldsymbol{F}$ is also applied, the classical and nonrelativistic motion equation reads

$$m\frac{d^2\boldsymbol{r}}{dt^2} = -e\boldsymbol{F} - e\frac{d\boldsymbol{r}}{dt}\times\boldsymbol{B} - \frac{ke^2\boldsymbol{r}}{r^3}, \tag{1}$$

where $k = 1/(4\pi\epsilon_0)$ is Coulomb's constant. This is a conservative system and the electron energy is given by

$$\frac{m}{2}\left(\frac{d\boldsymbol{r}}{dt}\right)^2 + e\boldsymbol{F}\cdot\boldsymbol{r} - \frac{ke^2}{r} = E. \tag{2}$$

In the present work the focus is on the orbits described by the electron after it launches from the close vicinity of the positive charge. The aim is to investigate the trajectories that return to the same vicinity. This is because they lead to the so-called quasi-Landau resonances [28] in the optical spectrum of atoms, where the initial state of the transitions is a highly localized state.

The motion equation is numerically solved for the positive charge at the origin of coordinates. In order to soften the singularity in the Coulomb term, semiparabolic coordinates u and v and a scaled time τ are introduced [29,30]. These coordinates are given by

$$x = \lambda uv\cos(\phi), \quad y = \lambda uv\sin(\phi),$$
$$z = \frac{\lambda}{2}(u^2 - v^2), \tag{3}$$

where ϕ is the azimuth and

$$\lambda = \sqrt[3]{\frac{4\pi^2 ke^2}{m\omega_c^2}} \tag{4}$$

is a convenient unit of length. Therefore, the distance to the origin is $r = \frac{\lambda}{2}(u^2 + v^2)$. The scaled time is given by

$$t = T_c\int_0^\tau \frac{r}{\lambda}\,d\tau, \tag{5}$$

where $T_c = 2\pi/\omega_c$ is the cyclotron period.

To be concrete, the magnetic field is chosen along the positive direction of the z axis, i.e., $\boldsymbol{B} = (0,0,B)$, with $B > 0$. The electric field will be given by $\boldsymbol{F} = F(\sin(\psi),0,\cos(\psi))$, where F is the intensity and $0 \leqslant \psi \leqslant \pi$. The motion equation (1) leads to

$$\ddot{u} = \frac{u\epsilon}{2} - \pi^2u^3v^2w - \pi^2uv^4(1-w)w - \frac{f}{2}u^3\cos(\psi) - \frac{f}{4}v(3u^2+v^2)\sin(\psi)\cos(\phi), \tag{6}$$

$$\ddot{v} = \frac{v\epsilon}{2} - \pi^2u^4v(1-w)w - \pi^2u^2v^3w - \frac{f}{4}u(u^2+3v^2)\sin(\psi)\cos(\phi) + \frac{f}{2}v^3\cos(\psi), \tag{7}$$

and

$$\dot{\phi} = 2\pi\, w\, r/\lambda, \tag{8}$$

where $\epsilon = 4\pi^2E/(m\omega_c^2\lambda^2)$, $w = (d\phi/dt)/\omega_c$, $f = 4\pi^2Fe/(m\omega_c^2\lambda)$, and

$$\dot{w} = \frac{f(u^2+v^2)\sin(\psi)\sin(\phi)}{4\pi uv} + (1-2w)\left(\frac{\dot{u}}{u} + \frac{\dot{v}}{v}\right). \tag{9}$$

Accordingly, Eq. (2) takes the form

$$\frac{(\dot{u})^2}{2} + \frac{(\dot{v})^2}{2} + \frac{\pi^2}{2}u^2v^2w^2(u^2+v^2) - \frac{\epsilon}{4}(u^2+v^2) + \frac{f}{8}(u^4-v^4)\cos(\psi) + \frac{f}{4}uv(u^2+v^2)\sin(\psi)\cos(\phi) = \frac{1}{2}, \tag{10}$$

The electron launches essentially from the origin. Theoretically, since the present approach does not include relativistic effects, the initial distance to the origin cannot be too small. For moderate energy values, i.e., for $|E| \ll mc^2$, such a distance should be much larger than $2ke^2/(mc^2) \approx 5.6$ fm. This is fairly small in comparison with the size of the hydrogen atom. Therefore, in the numerical calculations, one may take the initial position as $u = v = 0$.

The direction of the initial velocity is given by the polar angle θ and the azimuth ϕ. Since the initial electron position is the origin of coordinates, Eq. (10) leads to $\dot{u}^2 + \dot{v}^2 = 1$. Therefore, one may take $\dot{u} = \cos(\theta/2)$ and $\dot{v} = \sin(\theta/2)$. The singularity in Eq. (9) is avoided by taking $w = 1/2$ at $t = 0$. Thus the initial value of $\dot{w}$ is $f\sin(\psi)\sin(\phi)/[2\pi\sin(\theta)]$.

This method of scaling the equations and utilizing semiparabolic coordinates has been used in the special cases of pure magnetic fields and parallel electric and magnetic fields for several decades. In the case of crossed electric and magnetic

fields, due to the loss of rotational symmetry in the system, this method has been confined to analyzing the 2D hydrogen atom [25–27]. In the 3D hydrogen atom, other methods such as combining the Kustaanheimo-Stiefel transformation with a time-dilation variable in a four-dimensional representation have been required. Here we show that scaling of the equations, and semiparabolic coordinates, which had been predominantly limited to use in special cases with rotational symmetry, can also be generalized for arbitrary orientation of electric and magnetic fields in the 3D hydrogen atom.

A. Parallel fields

The electric field is parallel to the magnetic field when $\psi = 0$. In this case, w remains equal to $1/2$. This corresponds to a rotation around the z axis at the Larmor frequency. Because of symmetry, the initial value of ϕ does not affect the shape and the duration of the trajectories. Taking zero as the initial value of ϕ, one finds $\phi = \omega_c t/2$,

$$\ddot{u} = \frac{u\epsilon}{2} - \frac{\pi^2}{2}u^3v^2 - \frac{\pi^2}{4}uv^4 - \frac{f}{2}u^3 \tag{11}$$

and

$$\ddot{v} = \frac{v\epsilon}{2} - \frac{\pi^2}{4}u^4v - \frac{\pi^2}{2}u^2v^3 + \frac{f}{2}v^3, \tag{12}$$

which match equations published in Ref. [7] except for differences in scaling. The energy conservation equation now reads

$$\frac{(\dot{u})^2}{2} + \frac{(\dot{v})^2}{2} + \frac{\pi^2}{8}u^2v^2(u^2+v^2) - \frac{\epsilon}{4}(u^2+v^2) + \frac{f}{8}(u^4 - v^4) = \frac{1}{2}. \tag{13}$$

B. Crossed fields

The crossed-fields configuration corresponds to $\psi = \pi/2$. In this case the equations for u, v, and w are

$$\ddot{u} = \frac{u\epsilon}{2} - \pi^2u^3v^2w - \pi^2uv^4(1-w)w - \frac{f}{4}v(3u^2+v^2)\cos(\phi), \tag{14}$$

$$\ddot{v} = \frac{v\epsilon}{2} - \pi^2u^4v(1-w)w - \pi^2u^2v^3w - \frac{f}{4}u(u^2+3v^2)\cos(\phi), \tag{15}$$

and

$$\dot{w} = \frac{f(u^2+v^2)\sin(\phi)}{4\pi uv} + (1-2w)\left(\frac{\dot{u}}{u} + \frac{\dot{v}}{v}\right). \tag{16}$$

These equations of motion provide a simpler framework for the calculation of closed classical orbits than had previously been available in the crossed-fields configuration.

III. NUMERICAL RESULTS AND DISCUSSION

In the present work, the calculations are performed with a uniform step of 6" for θ. In all cases the electron energy is given by $\epsilon = 0$ unless stated otherwise.

TABLE I. The launching angle θ, the period T, and the return and maximum distances, for different values of the parallel electric-field intensity f. There are two almost closed orbits for most field strengths.

Orbit index	f	θ (deg)	T/T_c	$r_{\rm ret}/\lambda$	$r_{\rm max}/\lambda$
1	0.00	90.0	0.666667	1.8×10^{-32}	0.587368
	0.01	89.869	0.666666	1.3×10^{-8}	0.587367
	0.10	88.701	0.666627	1.2×10^{-8}	0.587312
	1.00	76.8383	0.662708	2.8×10^{-10}	0.581802
2	0.00	53.8317	1.57087	1.1×10^{-13}	0.707072
		126.168	1.57087	1.1×10^{-13}	0.707072
	0.01	53.577	1.57146	8.9×10^{-9}	0.708243
		125.914	1.57023	9.7×10^{-9}	0.705907
	0.10	51.219	1.57707	9.4×10^{-8}	0.719625
		123.678	1.56452	6.9×10^{-8}	0.696089
	1.00	12.17	1.62649	7.7×10^{-12}	0.955875
		104.915	1.50185	7.4×10^{-10}	0.633792
3	0.00	42.81	2.58188	2.9×10^{-9}	1.10748
		137.19	2.58188	2.9×10^{-9}	1.10748
	0.01	42.43	2.5831	2.8×10^{-8}	1.11103
		136.814	2.58068	9.9×10^{-9}	1.10396
	0.10	38.831	2.59346	7.5×10^{-8}	1.14398
		133.583	2.56998	6.6×10^{-8}	1.07352
	1.00	–	–	–	–
		109.787	2.44959	1.3×10^{-7}	0.857887
4	0.00	63.65	2.14518	4.5×10^{-8}	0.642937
		116.35	2.14518	4.5×10^{-8}	0.642937
	0.01	63.414	2.14512	7.8×10^{-8}	0.643456
		116.116	2.14514	8.3×10^{-8}	0.643477
	0.10	61.271	2.1444	8.9×10^{-8}	0.648843
		114.031	2.14439	7.9×10^{-8}	0.648857
	1.00	36.4983	2.04661	5.1×10^{-11}	0.724737
		94.7917	2.04663	4.0×10^{-9}	0.724763

A. Parallel fields

Table I presents the values of the launching angle θ, orbit period, return distance, and maximum distance for several scaled field values. In the absence of the electric field, i.e., for $f = 0$, the orbits correspond to the first four trajectories in Fig. 8 of Ref. [5]. The orbit periods would correspond to peaks in the Fourier transform of experimental spectra showing a correspondence between classical orbits and oscillations observed in the spectrum. The maximum distance of the orbit is large enough to justify the use of classical physics to produce accurate results and would also give an indication of the density of hydrogenic atoms required to consider every atom and associated electron orbit to be isolated.

Figure 1(a) is representative of a hydrogen atom in a static magnetic field which is a known chaotic system. However, over short time frames (less than $5T_c$ for the purposes of this work), pockets of stability exist in the form of electron orbits which return to the nucleus [5]. The local minima of the distance to the origin along the orbit, as a function of the launch distance, are depicted as dots in the figure. This results in bundles of almost closed orbits as shown in Fig. 1.

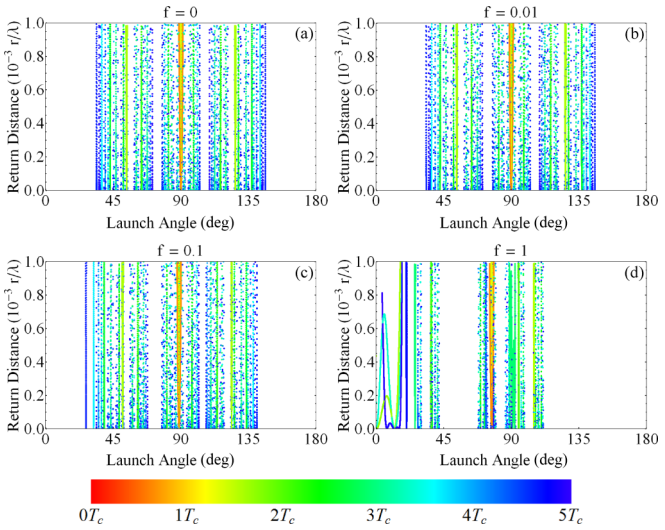

FIG. 1. The return distance to the nucleus as a function of launch polar angle for scaled parallel fields (a) $f = 0$, (b) $f = 0.01$, (c) $f = 0.1$, and (d) $f = 1$. Data points are shaded according to their orbital period in the range 0–$5T_c$ as indicated by the bar at the bottom of the figure. This convention will be adopted throughout the paper.

The results given in Table I represent the local minima of the distance to the nucleus corresponding to the bundle centers. The more stable an orbit, the more neighboring points appear [5] and the larger the bundle. This is dependent on how the angular distribution is sampled numerically. However, for any constant angular step size, the stability of the orbits relative to one another will remain essentially constant. The orbit located at a 90° launch angle in Fig. 1(a) is the first orbit identified by Garton and Tomkins [31] (hereafter referred to as the GT orbit), with the angular spectrum of orbits being symmetric with respect to $\theta = 90°$. The addition of a weak electric field in the direction of the magnetic field, as shown in panel (b), only perturbs the system slightly and, from Table I, only produces small differences in the orbit periods. This small perturbation is enough to break the symmetry of the spectrum of orbits around the GT orbit, as depicted in the orbit periods depending on whether the orbit is launched above or below $\theta = 90°$. Experimentally, this may be observed as peaks in the Fourier transformed spectra beginning to split due to the differences in orbit periods. Increasing the strength of the electric field as shown in panels (c) and (d) leads to a more noticeable loss of symmetry around $\theta = 90°$. As the field is increased, orbits migrate to launch angles closer to the direction of the electric field. This larger perturbation of the electron orbits has a stronger effect on the orbit periods. It is interesting to note that the application of the electric field produces a new closed orbit at $\epsilon = 0$ associated with the Stark effect. For instance, if $f = 1$ and $\theta = 0°$, then the period of a straight trajectory is $T = 1.694\,43\,T_c$, with the maximum distance to the origin being $r_{\max} = \lambda$. As other orbits migrate further towards this part of the spectrum they interact and mix together with this new orbit. The transition from the magnetic to the electric-field dominated atomic spectrum has been studied by König *et al.* [6] and will be investigated more thoroughly in the next section. Figures depicting the orbits detailed in Table I are provided in the Supplemental Material [32].

1. Orbit mixing at intermediate and high fields

As was demonstrated earlier in Fig. 1, at scaled fields of approximately $f = 1$ an orbit orientated parallel to the applied fields appears with a period less than $5T_c$. This orbit becomes more stable as the electric field is increased. As was also pointed out earlier, the orbits which are present at low fields migrate to launch angles close to parallel as the electric field is increased. Eventually, a field is reached in which these orbits begin to mix with the new electric-field-induced orbit and interesting features present themselves in the calculations. This section will focus on scaled fields of $f = 0.8$–1.18, increasing the field in 0.02 steps, in order to gain an understanding of how these orbits mix with each other. At these scaled fields, in contrast to at weaker fields, there are large regions where closed orbits proliferate.

Figure 2 depicts the system at angles $\theta \sim 0°$ for scaled fields of $f = 0.8$–0.98. At $f = 0.8$, orbits associated with quasi-Landau oscillations have migrated towards angles close to parallel from those shown earlier in Fig. 1(a). The orbit on the far left of all figures is the electric-field-induced orbit related to the Stark effect. The orbits which disappear between $f = 0.8$ and $f = 0.82$ in the region of 15–20° are due to those orbits coming together, mixing, and then evolving to the point where no orbits return to within 0.001λ of the nucleus. This was observed by increasing the field in 0.001 increments (figures detailing this process are presented as Supplemental Material [32]). The discontinuity on the far right at $f = 0.8$ is due to the orbit period moving from below to above $5T_c$. Increasing the field to $f = 0.82$ shifts the orbits on the right of the figure closer to parallel and the discontinuity no longer appears due to the higher field constricting the orbit further and therefore reducing its period below $5T_c$. Present in the figures are parabolas of different curvature with the same minimum point; these correspond to multiples ("harmonics") of the same orbit. The higher the harmonic, the more sensitive the orbit is to changes in initial launching angle and therefore the sharper the parabola.

Increasing the field to $f = 0.84$, the orbits on the right-hand side of the figure are beginning to cluster together and become more stable as is illustrated when increasing the field again to $f = 0.86$. This effect is strongest in orbits with longer periods. A few orbits in the middle of the figures disappear between $f = 0.84$ and $f = 0.86$ due to reasons discussed previously for orbits disappearing between $f = 0.8$ and $f = 0.82$.

At $f = 0.88$ we begin to see the overlapping of orbits and at $f = 0.9$ these orbits begin to mix creating nonparabolic orbit dispersion patterns. There are quite a few discontinuities present in the calculations at these fields. However, as the field is increased further, these discontinuities evolve and represent the changing periods of the orbits around $5T_c$.

Increasing the field again to $f = 0.92$, previous discontinuities have been resolved due to the increase in field and orbits previously seen as separated are now linked to one another. At $f = 0.94$ this creates a significant area of stability ranging over ~15°. This represents quite a large range compared to the region covered by the most stable orbits at $f = 0$ (the GT orbit is stable over an angular range of ~3°). We would therefore expect such orbits to yield strong features in spectra at these

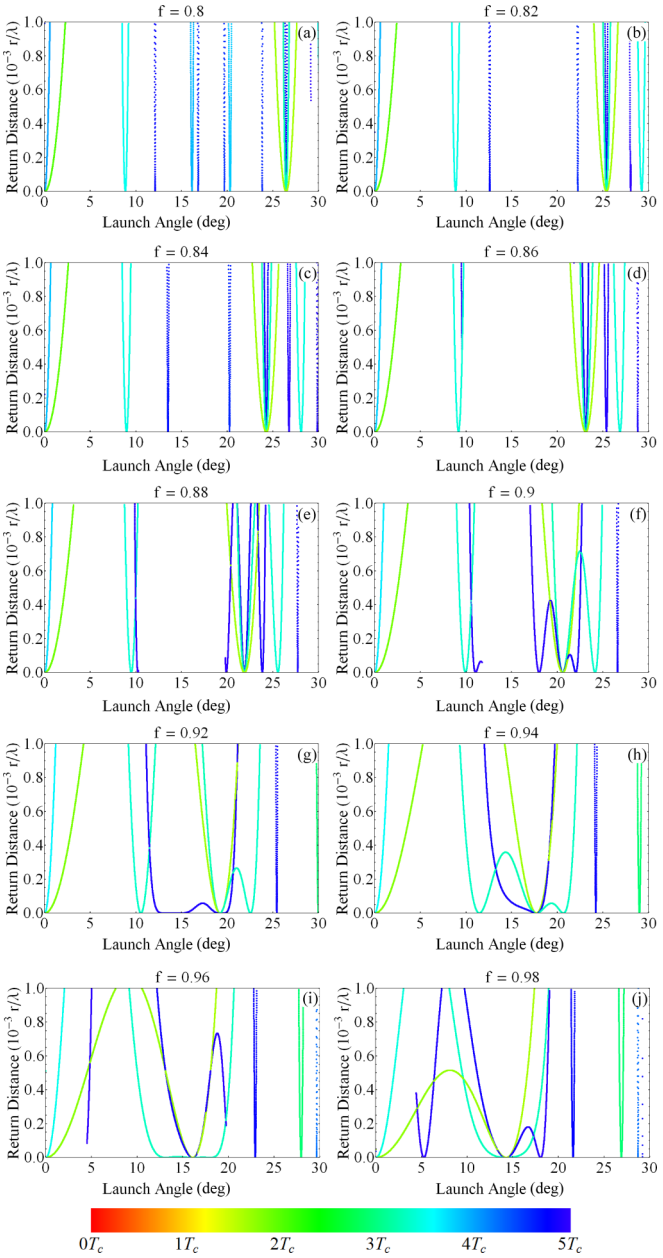

FIG. 2. Return distance to the nucleus as a function of launch polar angle for scaled parallel fields (a) $f = 0.8$, (b) $f = 0.82$, (c) $f = 0.84$, (d) $f = 0.86$, (e) $f = 0.88$, (f) $f = 0.9$, (g) $f = 0.92$, (h) $f = 0.94$, (i) $f = 0.96$, and (j) $f = 0.98$ at angles close to parallel to the applied fields.

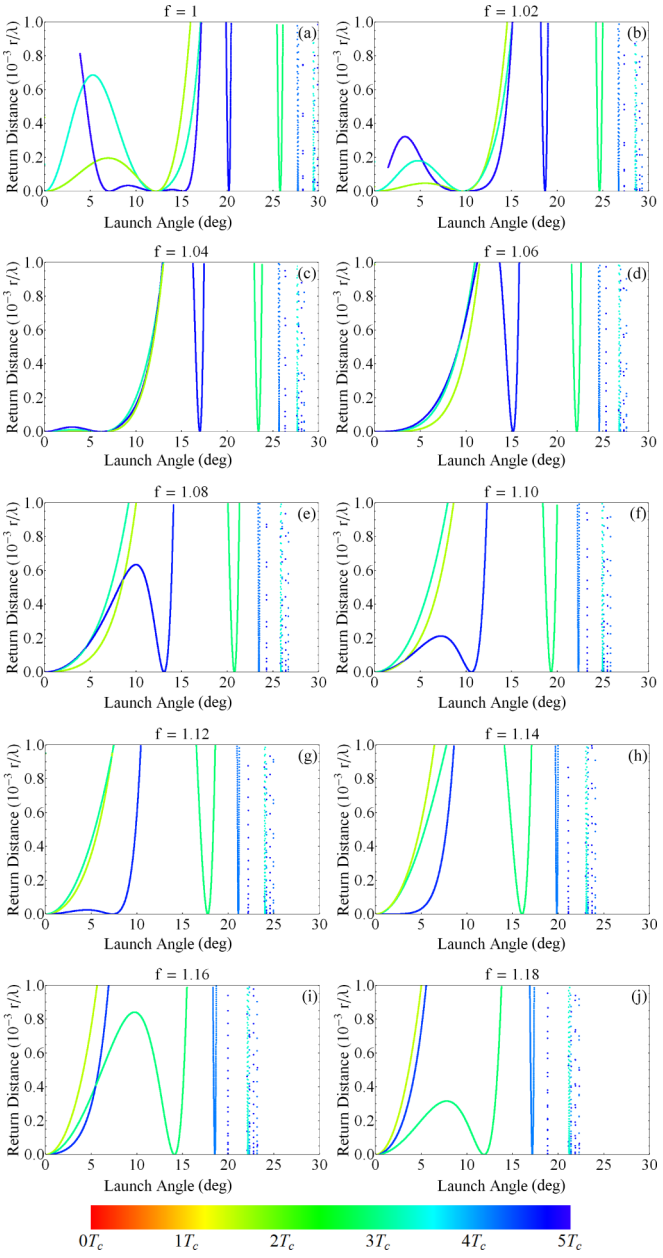

FIG. 3. Return distance to the nucleus as a function of launch polar angle for scaled parallel fields (a) $f = 1$, (b) $f = 1.02$, (c) $f = 1.04$, (d) $f = 1.06$, (e) $f = 1.08$, (f) $f = 1.10$, (g) $f = 1.12$, (h) $f = 1.14$, (i) $f = 1.16$, and (j) $f = 1.18$ at angles close to parallel to the applied fields.

fields. The electric-field-induced orbit is also expanding its range of stability with increasing field and therefore we would expect to see it becoming more influential in experimental results.

At fields of $f = 0.96$ and $f = 0.98$, the electric-field-induced orbit continues to increase in stability and the orbits associated with quasi-Landau oscillations continue shifting to launch angles closer to parallel resulting in the mixing of these orbits and extending further the region of stability in the spectrum of orbits. More orbits are also entering the panels on the right side as they continue to migrate as the field increases. Discontinuities are still present and evolving with increasing scaled field.

Figure 3 depicts the results at scaled fields of $f = 1$–1.18. At $f = 1$, the area of stability begins to contract back towards parallel as the orbits contributing to the right side of the large region of stability continue to shift towards parallel launch angles. Subsequently, we would expect the peaks observed in experimental data of Fourier transformed spectra to decrease in height as there is now a drop in the number of closed orbits over this scaled field range.

At $f = 1.04$ the electric-field-induced orbit and its associated harmonics all diverge from stability in essentially the same

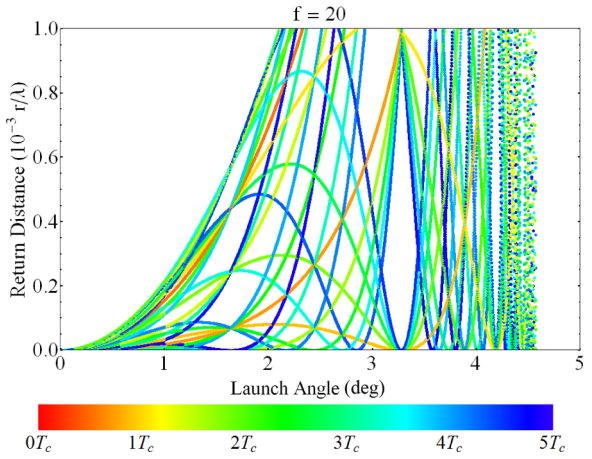

FIG. 4. Returning distance to the nucleus as a function of launch polar angle for scaled parallel field $f = 20$.

manner. This is contrary to anything which has been observed previously at other scaled fields as higher harmonics are expected to lose stability faster as is observed in the GT orbit and other quasi-Landau-associated orbits. Experimentally we might expect the peaks in a Fourier transformed spectra to have equal intensity for peaks corresponding to each harmonic. Increasing the field again to $f = 1.06$, we have another orbit significantly increasing in stability as it approaches the electric-field-induced orbit.

At $f = 1.08$ this orbit mixes with the electric-field-induced orbit creating a larger region of stability for that particular harmonic than for the other two. Again, this may be able to be observed in Fourier transformed spectra in their respective peak intensities. At $f = 1.10$, this region of stability decreases as the orbit which has mixed continues shifting towards parallel.

At fields of $f = 1.12$ and $f = 1.14$, the approach of another quasi-Landau-associated orbit to the electric-field-induced orbit is observed. As this new orbit approaches, it becomes increasingly more stable as seen by the widening of the parabola describing adjacent trajectories. The mixing of the orbit depicted at $f = 1.08$ is now unnoticeable at $f = 1.14$, as the region of stability of the electric-field-induced orbit contracts back towards its other harmonics.

At $f = 1.16$, the approaching orbit mixes with a different harmonic of the electric-field-induced orbit than was previously involved at $f = 1.08$. This mixing again leads to a large region of stability which may manifest itself in experimental measurements. Increasing the field again to $f = 1.18$, the mixing of the orbit with the electric-field-induced orbit follows the same pattern as was seen earlier in moving from $f = 1.08$ to $f = 1.10$.

Figure 4 shows all the closed orbits of the system for a scaled field $f = 20$. At this strong field, all quasi-Landau-associated orbits have migrated to launch angles close to $\theta = 0^\circ$ and are interacting with the electric-field-induced orbit and its associated harmonics. This represents a close to full transition from the chaotic regime at $f = 0$ to the regular regime at $f = \infty$. Therefore, we can conclude that the mixing of orbits which has been detailed represents the dynamics of the system shifting from one regime to the other.

TABLE II. The launching angle θ, the period T, and the return and maximum distances, for different values of the classical energy ϵ at a fixed scaled parallel field of $f = 1$.

Orbit index	ϵ	θ (deg)	T/T_c	$r_{\rm ret}/\lambda$	$r_{\rm max}/\lambda$
1	0	76.84	0.662706	5.0992×10^{-9}	0.581801
	1	78.714	0.742808	1.49022×10^{-8}	0.695772
	2	80.028	0.798498	6.10091×10^{-9}	0.804591
	3	80.994	0.837343	6.05821×10^{-9}	0.906482
	4	81.735	0.865182	5.39586×10^{-8}	1.00157
2	0	12.271	1.62543	3.62469×10^{-7}	0.955163
		104.915	1.50185	6.83174×10^{-8}	0.633792
	1	40.616	1.69678	3.78973×10^{-8}	0.912468
		97.383	1.59973	1.27222×10^{-8}	0.725303
	2	51.786	1.75212	5.91534×10^{-8}	0.945133
		93.444	1.67696	1.36753×10^{-7}	0.822794
	3	58.362	1.79414	2.65158×10^{-8}	1.01163
		91.28	1.73488	3.12071×10^{-8}	0.918555
	4	62.717	1.82605	1.96283×10^{-8}	1.08605
		90.018	1.77817	1.48121×10^{-7}	1.01009
3	0	–	–	–	–
		109.786	2.44946	4.93364×10^{-8}	0.857853
	1	–	–	–	–
		101.177	2.54127	4.45631×10^{-8}	0.906536
	2	32.996	2.77808	1.29848×10^{-5}	1.65875
		96.379	2.61708	9.41017×10^{-7}	0.965357
	3	43.622	2.812	1.05115×10^{-7}	1.69403
		93.577	2.67684	9.14176×10^{-7}	1.03068
	4	50.195	2.83834	6.47719×10^{-9}	1.73337
		91.853	2.7236	9.47386×10^{-7}	1.09936
4	0	36.498	2.0466	7.54841×10^{-8}	0.72474
		94.792	2.04661	6.97346×10^{-8}	0.724742
	1	48.103	2.3691	4.15814×10^{-8}	0.819641
		91.368	2.36911	3.85737×10^{-8}	0.81967
	2	56.239	2.52946	7.76836×10^{-8}	0.899922
		89.326	2.52947	3.18742×10^{-9}	0.899916
	3	61.533	2.62874	6.83799×10^{-7}	0.982804
		88.209	2.62876	1.46014×10^{-7}	0.982884
	4	65.179	2.69622	5.1662×10^{-7}	1.0652
		87.589	2.69626	2.46447×10^{-7}	1.06528

2. *Intermediate positive energy*

In 2009, the diamagnetic Kepler problem was observed in the semiconductor environment [22]. Five years later, we have shown [23] that a scaled energy above the ionization threshold provides a good match between theory and experiment. This is due to the spectral oscillations occurring far beyond the ionization threshold. Much work in the literature regarding elemental gases has been focused in the region of $\epsilon \leqslant 0$. We look here to investigate the effect positive energy values have on both the orbits and the system as a whole in the high-field regime of $f = 1$. Table II gives the values of the launching angle θ, orbit period, return distance, and the maximum distance for positive integer values of the classical scaled energy ϵ up to $\epsilon = 4$ (the energy identified as being the best match to experimental data [23]).

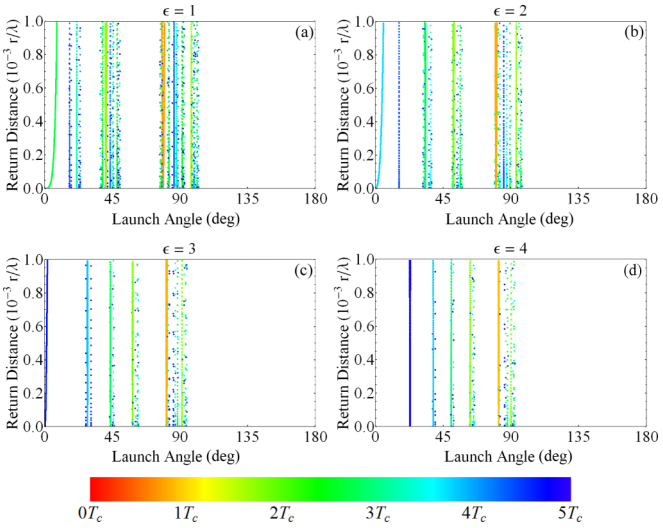

FIG. 5. The return distance to the nucleus as a function of launch polar angle for scaled parallel field $f = 1$ and a classical energy of (a) $\epsilon = 1$, (b) $\epsilon = 2$, (c) $\epsilon = 3$, and (d) $\epsilon = 4$.

From Table II, the orbit periods do change substantially when varying the energy. This is important when moving into the semiconductor environment with the only experimental results being explained by orbits with positive intermediate energies. Figure 5 shows the spectrum of orbits as the scaled energy is increased in integer steps. The results for $\epsilon = 0$ were shown earlier in Fig. 1(d). Many of the orbits present at $\epsilon = 0$ no longer have periods less than $5T_c$ at higher energies leaving only a few stable orbits. Orbit mixing no longer occurs as the energy is increased from $\epsilon = 0$ to 1 and, as it is increased to a value of $\epsilon = 4$, the electric-field orbit disappears from the results as its period now exceeds the $5T_c$ threshold in the calculations. Figures depicting the orbits detailed in Table II are presented as Supplemental Material [32].

As is to be expected, Figs. 15–28 of the Supplemental Material [32] show that increasing the classical energy has the opposite effect to increasing the scaled field. Increasing the scaled field leads to orbits becoming constricted and launch angles migrating towards the direction of the applied fields; here the orbits are enlarged and launch angles migrate back towards $\theta = 90°$. As the orbits are being enlarged under these conditions, semiconductor samples need to be very pure in order for doping sites to be regarded as isolated for the observation of quasi-Landau oscillations [24].

B. Crossed fields

This field configuration lacks the rotational symmetry of the pure magnetic field and parallel fields cases and therefore calculations should be performed for different values of the polar angle θ and the azimuth ϕ of the launching velocity. While θ varies from 0° to 180°, ϕ goes from 0° to 360°. There still remain three symmetries in the system as discussed by Bartsch *et al.* [17]. The first is a reflection in the x-y plane, the second is a combination of time reversal and a reflection in the x-z plane, and the third is the combination of the first two symmetries.

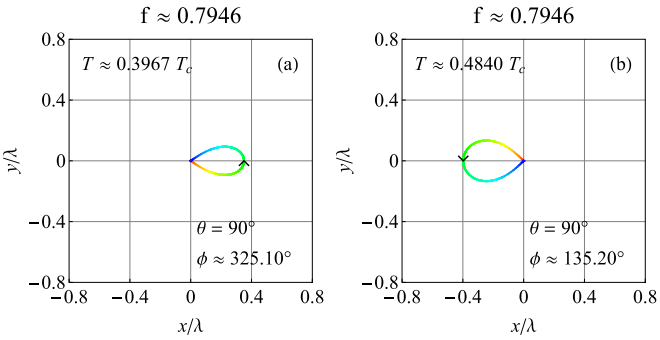

FIG. 6. The shape of a closed orbit on the x-y plane for scaled energy $\epsilon \approx -1.9972$ and scaled crossed field $f \approx 0.7946$, when the electron is launched at $\theta = 90°$ and (a) $\phi \approx 325.10°$, (b) $\phi \approx 135.20°$. The shading of the curve represents changing time as the electron describes the essentially closed path in the direction of the arrow shown on the orbit.

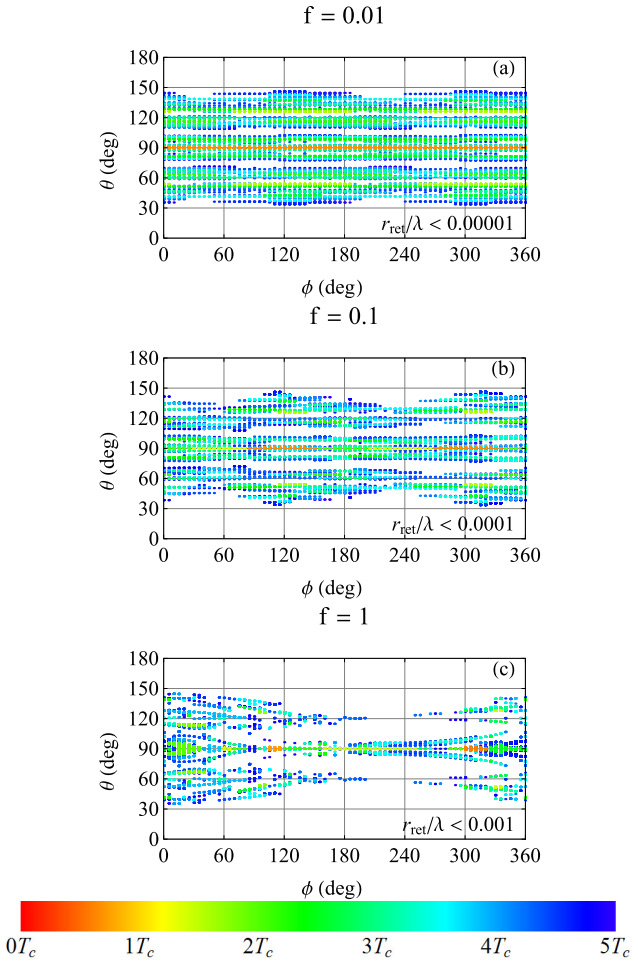

FIG. 7. The relation between the polar angle θ and the azimuth ϕ of the launching velocity of essentially closed orbits of an electron with energy $\epsilon = 0$, in the presence of crossed electric and magnetic fields along the directions of the x and z axes, respectively. Panels (a)–(c) are for electric-field strength $f = 0.01$, $f = 0.1$, and $f = 1$, respectively. Orbits whose scaled returning distance, r_{ret}/λ, is larger than (a) 0.00001, (b) 0.0001, and (c) 0.001 are not shown.

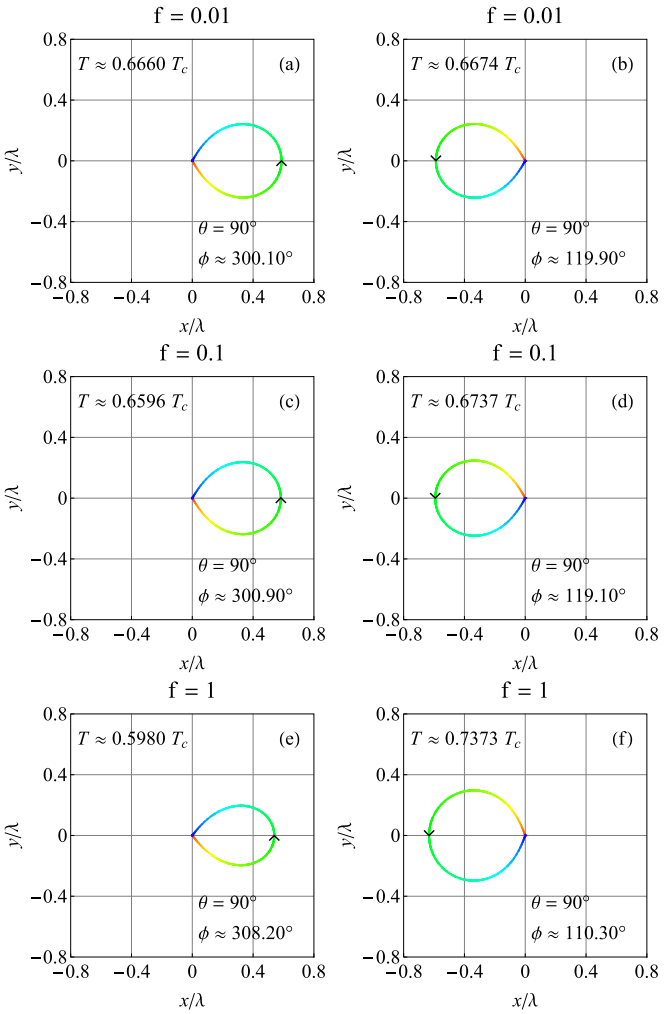

FIG. 8. The shapes of the plane closed orbits that evolve from the Garton-Tomkins orbit in the crossed fields, for $\epsilon = 0$, and (a), (b) $f = 0.01$, (c), (d) $f = 0.1$, and (e), (f) $f = 1$.

We first show that our simplified method is able to produce the same results as those reported by Rao *et al.* [20]. To calculate the orbits displayed in Fig. 4 of that work, we must convert the energy and electric-field values to the units introduced above. The values of ϵ and $\tilde{f}$ in Ref. [20] should be multiplied by $(2\pi)^{2/3}$ and $(2\pi)^{4/3}$, respectively. The calculations for $\epsilon = -1.997\,177\,713\,650\,031\,3$ and $f = 0.794\,639\,734\,100\,187\,3$ yield the orbits displayed in Fig. 6. The shapes of the orbits are in good agreement with Figs. 4(a) and 4(b) of Ref. [20]. The sizes of the orbits in the present calculation are smaller due to the use of a unit of length which is $(2\pi)^{2/3}$ times larger.

The overall dependence of the launching direction and the duration of the closed orbits on the strength of the electric field is displayed in Fig. 7. As the field strength increases from panel (a) to (c), the dependence of the polar angles and duration of closed orbits on the azimuth becomes more apparent. The reflection symmetry with respect to the x-y plane, i.e., $\theta = 90°$, is quite evident. Moreover, the orbits of shorter duration are launched on the symmetry plane and evolve from the GT orbits. The evolution may be understood by analyzing Fig. 8,

TABLE III. The launching angle θ, the period T, and the return and maximum distances, for different values of the crossed electric-field intensity f. The launching azimuth is $\phi = 0°$.

Orbit index	f	θ (deg)	T/T_c	$r_{\rm ret}/\lambda$	$r_{\rm max}/\lambda$
1	0.00	90.0	0.666667	1.8×10^{-32}	0.587368
	0.01	90.0	0.666003	2.3×10^{-6}	0.586742
	0.10	90.0	0.660125	2.2×10^{-4}	0.581168
	1.00	90.0	0.607811	1.4×10^{-2}	0.530252
2	0.00	53.8317	1.57087	1.1×10^{-13}	0.707072
	0.01	53.7933	1.56928	8.3×10^{-6}	0.706661
	0.10	53.4717	1.55474	7.5×10^{-4}	0.702828
	1.00	52.085	1.37526	1.8×10^{-2}	0.652981
3	0.00	42.81	2.58188	2.9×10^{-9}	1.10748
	0.01	42.77	2.57934	2.2×10^{-5}	1.10667
	0.10	42.445	2.55462	1.9×10^{-3}	1.09839
	1.00	40.9933	2.25026	1.8×10^{-4}	0.989591
4	0.00	63.65	2.14518	4.5×10^{-8}	0.642937
	0.01	63.6467	2.14087	6.0×10^{-7}	0.642202
	0.10	63.635	2.10329	2.6×10^{-5}	0.636107
	1.00	64.9833	1.84521	4.3×10^{-3}	0.625781

where the two orbits having minimum returning distance are displayed for $f = 0.01$, $f = 0.1$, and $f = 1$. The duration of the closed orbits in panels (a), (c), and (e) is less than $\frac{2}{3}T_c$. As the electric-field strength increases, both the duration and the size of the orbit decrease. The orbits in panels (b), (d), and (f) last more than $\frac{2}{3}T_c$ and display the opposite dependence on the field strength.

We now consider the cases where the electron is launched on the vertical semiplane given by $y = 0$ and $x \geqslant 0$, i.e., $\phi = 0$. The parameters of the orbits that evolve from the main orbits in the absence of the electric field are given in Table III.

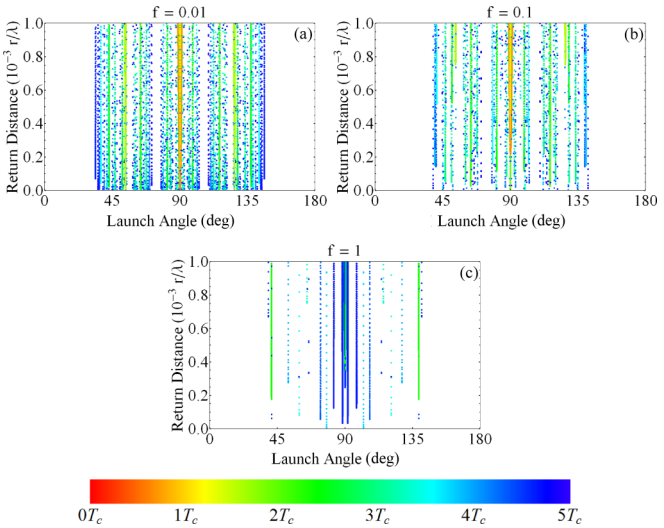

FIG. 9. The return distance against launch polar angle in crossed fields at $\phi = 0°$ and for scaled fields of (a) $f = 0.01$, (b) $f = 0.1$, and (c) $f = 1$.

TABLE IV. The launching angle θ, the period T, and the return and maximum distances, for different values of the crossed electric-field intensity f. The launching azimuth is $\phi = 90^\circ$.

Orbit index	f	θ (deg)	T/T_c	$r_{\rm ret}/\lambda$	$r_{\rm max}/\lambda$
1	0.00	90.0	0.666667	1.8×10^{-32}	0.587368
	0.01	90.0	0.667098	7.6×10^{-7}	0.58756
	0.10	90.0	0.671077	7.3×10^{-5}	0.589323
	1.00	90.0	0.720405	4.2×10^{-3}	0.610131
2	0.00	53.8317	1.57087	1.1×10^{-13}	0.707072
	0.01	53.8217	1.57189	5.3×10^{-6}	0.707486
	0.10	53.7233	1.58232	4.8×10^{-4}	0.711371
	1.00	52.6233	1.76554	2.2×10^{-3}	0.761754
3	0.00	42.81	2.58188	2.9×10^{-9}	1.10748
	0.01	42.8	2.58403	1.3×10^{-5}	1.10807
	0.10	42.6967	2.60742	1.0×10^{-3}	1.11434
	1.00	42.87	2.89857	4.4×10^{-2}	1.17774
4	0.00	63.65	2.14518	4.5×10^{-8}	0.642937
	0.01	63.6617	2.14349	1.2×10^{-5}	0.643068
	0.10	63.7717	2.13007	1.1×10^{-3}	0.644824
	1.00	63.615	2.14893	6.6×10^{-2}	0.673262

Figure 9 depicts how the system evolves as the scaled field is varied for $\phi = 0^\circ$. The results for $f = 0$ were shown earlier in Fig. 1(a). As was the case for parallel fields, a weak electric field only yields a small perturbation in the results as shown in Table III. As the field is increased further, fewer orbits return close to the nucleus. This is seen by the relative absence of orbits returning within a distance of 0.0002λ in comparison to the parallel-fields case. In this configuration, the plane containing the orbit which is identified as the GT orbit at $f = 0$ is now parallel to the electric field which changes the behavior of this orbit substantially. At $f = 0.1$ it is seen that the first harmonic is no longer returning as close to the nucleus as at lower fields and at $f = 1$ it no longer returns to within the 0.001λ threshold. Figures depicting the orbits detailed in Table III are presented as Supplemental Material [32].

Table IV and Fig. 10 are for launching azimuth $\phi = 90^\circ$. Figure 10 shows how the system changes as the scaled field is varied for launch angles perpendicular to the applied electric field, i.e., $\phi = 90^\circ$. The results for $f = 0$ were shown earlier in Fig. 1(a). As was the case in the parallel fields and $\phi = 0^\circ$ cases, a weak electric field only yields a small perturbation in the results as shown in Table IV. Increasing the electric field to a scaled field of $f = 1$, there appear to be no short period orbits which return within 0.001λ of the nucleus and the orbits which do appear have quite low stability. Therefore, the oscillations in the spectrum linked to these orbits would be quite weak compared to those depicted for $\phi = 0^\circ$. Figures depicting the orbits detailed in Table IV are presented in the Supplemental Material [32].

It should be stressed that the present method is not appropriate for the study of orbits launched near either $\theta = 0^\circ$ or $\theta = 180^\circ$ in crossed fields. Therefore, orbits of this kind that have been reported by Rao *et al.* [20,21] have not been obtained here. Nevertheless, such orbits are not very stable and should not manifest themselves in the optical spectra.

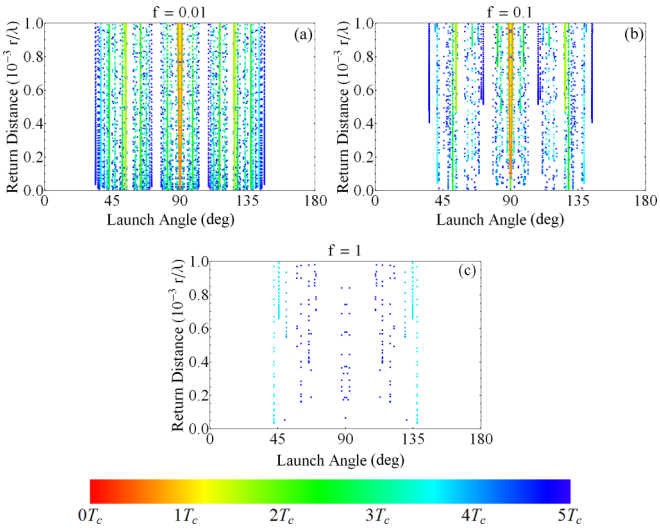

FIG. 10. The return distance against launch polar angle in crossed fields at $\phi = 90^\circ$ and for scaled fields of (a) $f = 0.01$, (b) $f = 0.1$, and (c) $f = 1$.

IV. CONCLUSIONS

The closed orbits of an electron interacting with a positive unit charge in the presence of magnetic and electric fields have been calculated in a simpler manner than has been reported previously for the cases of parallel and crossed-field configurations. Such trajectories may manifest themselves in the optical spectrum of an atomic system. The calculations show the evolution of the orbits reported by Du and Delos [5], as the electric-field intensity and classical energy are increased. Small changes are seen for $f \leqslant 0.1$. However, at higher fields the orbits do undergo significant changes in size, shape, and duration.

In the parallel fields geometry, the emergence of the electric-field-induced orbit associated with the Stark effect, and the incremental increase of the scaled field, leads to some complex behavior as quasi-Landau-associated orbits interact with this Stark orbit at launching angles close to parallel with the external fields. Large regions of the system facilitate closed orbits in this region which are not seen in other regions or associated with other orbits. We expect this large range of stability to become more dominant in comparison to the rest of the orbit spectrum in experimental results as the scaled field is increased and orbits continue to migrate to launch angles closer to the field direction. Since this orbit mixing shows similar behavior to the system at extreme electric-field strength, which is known to be a regular system, this orbit mixing may provide an indication of the system moving from chaotic to regular dynamics.

The introduction of a finite positive energy, which has been shown previously to be important in the semiconductor environment [23,24], also has a large impact on the size, shape, and period of the closed orbits but in the opposite manner to

increasing the scaled field. While a finite positive energy leads to an expansion of the orbits' size, shape, and their associated periods, increasing the scaled field generally constricts the orbits and their periods.

In the presence of crossed fields, the rotational symmetry of the set of nearly closed orbits is broken by the electric field. The Garton-Tomkins orbit splits into a pair of orbits whose evolution occurs in opposite ways as the field strength increases. The duration and the size of one of them decreases in the range of intensities under investigation. In a sufficiently strong field, such a splitting should be apparent in the Fourier transform of the optical spectrum.

We expect our detailed analysis of the closed orbits to encourage and partially explain further experimental investigation of quasi-Landau resonances in both atomic and shallow-impurity systems.

ACKNOWLEDGMENTS

The work was supported by the Australian Research Council and the University of Wollongong (under the UIC International Links Scheme). A.B.-A. is thankful to the University of Wollongong for warm hospitality and acknowledges the financial support of the Brazilian Agencies FAPESP (Grant No. 2014/23833-0) and CNPq (Grant No. 310975/2014-0).

[1] D. Delande, Phys. Scr. **T34**, 52 (1991).
[2] J. Main and G. Wunner, J. Phys. B **27**, 2835 (1994).
[3] J. Main, G. Wiebusch, A. Holle, and K. H. Welge, Phys. Rev. Lett. **57**, 2789 (1986).
[4] A. Holle, J. Main, G. Wiebusch, H. Rottke, and K. H. Welge, Phys. Rev. Lett. **61**, 161 (1988).
[5] M. L. Du and J. B. Delos, Phys. Rev. A **38**, 1896 (1988).
[6] A. König, J. Neukammer, K. Vietzke, M. Kohl, H. J. Grabka, H. Hieronymus, and H. Rinneberg, Phys. Rev. A **38**, 547 (1988).
[7] H. H. Fielding, J. Wals, W. J. van der Zande, and H. B. van Linden van den Heuvell, Phys. Rev. A **51**, 611 (1995).
[8] M. A. Iken, F. Borondo, R. M. Benito, and T. Uzer, Phys. Rev. A **49**, 2734 (1994).
[9] M. W. Beims and J. A. C. Gallas, Phys. Rev. A **62**, 043410 (2000).
[10] T. Topçu and F. Robicheaux, J. Phys. B **40**, 1925 (2007).
[11] R. R. Freeman, N. P. Economou, G. C. Bjorklund, and K. T. Lu, Phys. Rev. Lett. **41**, 1463 (1978).
[12] M. Courtney, H. Jiao, N. Spellmeyer, D. Kleppner, J. Gao, and J. B. Delos, Phys. Rev. Lett. **74**, 1538 (1995).
[13] M. Courtney, N. Spellmeyer, H. Jiao, and D. Kleppner, Phys. Rev. A **51**, 3604 (1995).
[14] G. Wiebusch, J. Main, K. Krüger, H. Rottke, A. Holle, and K. H. Welge, Phys. Rev. Lett. **62**, 2821 (1989).
[15] C. Neumann, R. Ubert, S. Freund, E. Flöthmann, B. Sheehy, K. H. Welge, M. R. Haggerty, and J. B. Delos, Phys. Rev. Lett. **78**, 4705 (1997).
[16] S. Freund, R. Ubert, E. Flöthmann, K. Welge, D. M. Wang, and J. B. Delos, Phys. Rev. A **65**, 053408 (2002).
[17] T. Bartsch, J. Main, and G. Wunner, Phys. Rev. A **67**, 063410 (2003).
[18] T. Bartsch, J. Main, and G. Wunner, Phys. Rev. A **67**, 063411 (2003).
[19] F. Schweiner, J. Main, H. Cartarius, and G. Wunner, Phys. Rev. E **91**, 012915 (2015).
[20] J. Rao, D. Delande, and K. T. Taylor, J. Phys. B **34**, L391 (2001).
[21] J. Rao and K. T. Taylor, J. Phys. B **35**, 2627 (2002).
[22] Z. Chen, W. Zhou, B. Zhang, C. H. Yu, J. Zhu, W. Lu, and S. C. Shen, Phys. Rev. Lett. **102**, 244103 (2009).
[23] A. Bruno-Alfonso, C. Bleasdale, G. V. B. de Souza, and R. A. Lewis, Phys. Rev. A **89**, 043425 (2014).
[24] C. Bleasdale and R. A. Lewis, Phys. Status Solidi B **252**, 2657 (2015).
[25] M. J. Raković, T. Uzer, and D. Farrelly, Phys. Rev. A **57**, 2814 (1998).
[26] C. Jaffé, D. Farrelly, and T. Uzer, Phys. Rev. Lett. **84**, 610 (2000).
[27] C. Chandre, S. Wiggins, and T. Uzer, Phys. D (Amsterdam, Neth.) **181**, 171 (2003).
[28] A. R. Edmonds, J. Phys., Colloq. **31**, C4-71 (1970).
[29] D. Wintgen, J. Phys. B **20**, L511 (1987).
[30] W. Schweizer, R. Niemeier, H. Friedrich, G. Wunner, and H. Ruder, Phys. Rev. A **38**, 1724 (1988).
[31] W. R. S. Garton and F. S. Tomkins, Astrophys. J. **158**, 839 (1969).
[32] See Supplemental Material at http://link.aps.org/supplemental/10.1103/PhysRevA.93.023405 for figures displaying additional orbits and angular spectra.